

PCCP

Accepted Manuscript



This is an *Accepted Manuscript*, which has been through the Royal Society of Chemistry peer review process and has been accepted for publication.

Accepted Manuscripts are published online shortly after acceptance, before technical editing, formatting and proof reading. Using this free service, authors can make their results available to the community, in citable form, before we publish the edited article. We will replace this *Accepted Manuscript* with the edited and formatted *Advance Article* as soon as it is available.

You can find more information about *Accepted Manuscripts* in the [Information for Authors](#).

Please note that technical editing may introduce minor changes to the text and/or graphics, which may alter content. The journal's standard [Terms & Conditions](#) and the [Ethical guidelines](#) still apply. In no event shall the Royal Society of Chemistry be held responsible for any errors or omissions in this *Accepted Manuscript* or any consequences arising from the use of any information it contains.



PCCP

ARTICLE

Metal based bracken-like single sided dye sensitized solar cells with horizontal separation

Received 00th January 20xx,
Accepted 00th January 20xx

DOI: 10.1039/x0xx00000x

www.rsc.org/

F. Behrouznejad,^a N. Taghavinia,^{a,b,*} M. Pazoki,^c F. Tajabadi^d

One of the drawbacks of typical dye sensitized solar cells (DSCs) is the cost and rather high electrical resistance of the transparent conducting substrate. In the conventional sandwich type DSCs, only one of FTO substrates can be replaced by metal. Herein, we have investigated an all-metal-electrode single-sided DSC in which interpenetrated bracken-like Cr electrodes are created using photolithography, and mesoporous TiO₂ and Pt films are deposited on the laterally separated electrodes respectively. Thermal Pt deposition and electrodeposition methods are tried, and it is found that cyclic electrodeposition method provides selective Pt deposition at room temperature with a higher device performance. For the spacer layer that keeps the Pt electrode away from TiO₂ mesoporous layer, Cu or ZnO sacrificial layers and also TiO₂ or TiO₂/SiO₂ porous layers are implemented and optimum results are obtained for the TiO₂/SiO₂ layer. Champion device shows the current density of 8.47 mA/cm², open circuit voltage of 0.685 V and an efficiency of 2.44%. Open circuit voltage decay and electrochemical impedance spectroscopy of the cells demonstrate the formation of a high resistivity blocking layer, which is attributed to the chromium oxide formed during the thermal treatments. The efficiency can be further improved by developing low-temperature fabrication processes.

Introduction

Dye sensitized solar cells (DSC) utilize transparent conducting oxides (TCO) as the substrate for both cathode and anode sides. There have been many efforts to replace one of the TCO substrates with metal substrates in order to decrease the cost¹ and also reduce the series resistance of the cells. Two major disadvantages of metal substrates are the corrosion of metal in the iodine-based electrolyte of DSCs,²⁻⁴ as well as the opaque nature of metal which changes the transparency and hinder the possibility of two-side illumination of the cell. The easier structure for using metals in DSCs is replacing the counter-electrode substrate, normally FTO/glass or sometimes ITO/glass (FTO: F-doped tin oxide, ITO: indium tin oxide), with

metal foils or metal thin films, which makes no constraint for the optical design of the cell.⁴⁻⁶ However, for flexible cells the preferred structure is the replacement of photo-anode substrate with metal foils⁷⁻¹⁰ metal mesh¹¹⁻¹³ or thin films.¹⁴ Metals are favoured over plastics as flexible substrates due to higher temperature tolerance during the sintering process. In both cases of DSC with metal based photo-anode or counter-electrode, TCO substrate may cause some voltage loss due to the relatively high electrical resistance. Hence, for large area cells and solar modules, metal bus-bars with low series resistance are obligatory. Printing Ag paste is common in DSC modules. There are, however, two problems: The first is that Ag is not stable in the corrosive electrolyte of DSCs, so depositing a protective layer is essential. The second is that printed Ag shows usually higher resistance compared to dense electrodeposited Ag films with the same thickness. Using Ni bus-bars in dye solar modules is also reported; nevertheless it needs ITO/FTO over layer deposition for chemical protection of the metal,¹⁵ which is not an easy task. The ideal structure would be replacing both substrates by stable metal substrates. There are few reports on using metal mesh¹² or wire (i.e. Ti wires¹⁶) as the substrate of photo-anode. In these cases, the substrate of the counter-electrode can be replaced by a metal substrate. This structure has several manufacturing complexities such as complexity of the sealing, difficulty of assembling the electrodes (there is probability of contacting

^a Institute for Nanoscience and Nanotechnology, Sharif University of Technology, Tehran 14588, Iran.

^b Department of Physics, Sharif University of Technology, Tehran 14588, Iran Fax: +98-21-66022711; Tel: +98-21-6616 4532.

^c Department of Chemistry-Ångström Laboratory, Uppsala University, Box 523, SE-751 20 Uppsala, Sweden.

^d Nanotechnology and Advanced Materials Department, Materials and Energy Research Center, Karaj 31787-316, Iran.

Electronic Supplementary Information (ESI) available: Comparison of using different substrates (FTO, Ni and Cr) and different spacers between photo-anode and counter-electrode (Cu, Poly anilin, and ZnO) are shown in supplementary information. Details of fitting results of Nyquist plots related to monolithic bracken like DSCs with counter-electrodes prepared by electrodeposition Pt salt and doctor blading Pt paste are also reported. See DOI: 10.1039/x0xx00000x

lower part of mesh with the upper surface of metallic foil) and thick features of the mesh. These parameters make the fabrication process uncontrollable.

There are reports about producing the monolithic structures to overcome the complexity of assembling and replacing one of FTO substrates with carbon composite,^{17,18} conductive polymer composites (such as PEDOT composites)^{19,20} or metal thin films. Monolithic based DSCs with carbon composites as the counter-electrode, usually suffer from the low fill factor in which the carbon composite must keep high enough porosity to permit the electrolyte in, and at the same time be highly conductive. Therefore, the layer should be rather thick; i.e. 10-15 μm of carbon composite layer consisted of graphite for decreasing series resistance and conventionally carbon black and/or Pt as a catalyst material. Relatively low fill factor and high series resistance is one of the limiting factors for large area cells and modules based on these structures. Fu et al have reported a monolithic structure with sputtered Ti thin film as substrate for TiO₂, a ZrO₂ layer as spacer layer and the FTO/glass-Pt or Ti foil/Pt as counter-electrode.¹⁴ Earlier Fuke reported back contact DSC structure with conventionally separated electrodes, and glass/TiO₂ porous layer/Ti layer (deposited by sputtering method) as a photo-anode.^{21,22} In both structures, Ti layer cannot be thick and must be thin enough to have some holes in the structure to permit ionic diffusion. This demands highly controlled deposition and the final film is not as effective in reducing the series resistance due to the low thickness.

Here we introduce a single sided integrated metal based DSC with bracken shaped electrodes. We have already shown that electrodeposited Cr layer can be a good candidate for low-cost replacement of TCO substrates of photo-anode²³ and counter-electrode²⁴ in DSCs. Selective thin film deposition on patterned substrates is usually achieved using physical vapour deposition (PVD) and lithographic lift-off methods, that are expensive and time-consuming. Besides, deposition of films with micron thicknesses is usually a difficult task with PVD.²⁵ Selective deposition on integrated bracken like electrodes using low-cost electrochemical methods is a challenge that is studied in the current article. Different Pt deposition methods such as thermal deposition (drop-casting of H₂PtCl₆ solution or doctor-blading of H₂PtCl₆ paste), chemical reduction, constant voltage electrodeposition, and cyclic electrodeposition are investigated in order to selectively deposit the Pt nanoparticles on the bracken-like counter-electrode substrate. There are several reports about Pt-based counter-electrode in which Pt is deposited by different methods:²⁶ thermal deposition and chemical reduction,^{5,27-29} sputtering,³⁰⁻³² e-beam evaporation,³³ electrodeposition,³⁴⁻³⁷ or making composites of Pt and other materials.³⁸⁻⁴⁶ Herein the main concern is selective deposition

of Pt nanoparticles on one of the electrodes, without leaving Pt nanoparticles in the photo-anode structure; our results show that for this purpose the best method is cyclic electrodeposition method.

Results and discussion

In a single-sided DSC structure, the anode and cathode are laterally separated. The injected electrons in the TiO₂ mesoporous film are needed to travel both in the depth and also laterally in order to be captured by the anode electrode. This implies that electron diffusion length in these structures should be larger than the lateral electrode spacing. The reported values for electron diffusion length in TiO₂ or ZnO mesoporous layers are in the range of 7-30 μm in light intensities of down to 0.1 Sun.⁴⁷ It depends on the crystallinity and porosity of the mesoporous film.

On the other hand, the electrode separation may also hinder the ionic diffusion in the electrolyte. The critical parameters here are the diffusion coefficient of I₃⁻ species, as well as the concentration of I₃⁻ in the electrolyte. The diffusion coefficient of I₃⁻ (*D*_{I₃⁻) depends on the solution viscosity, for conventional solvents such as acetonitrile and valeronitrile is 1.5×10⁻⁵ cm²/sand for less volatile solvents (such as 1-Methyl-3-propylimidazolium iodide 3-methoxypropionitrile) ranges between 1.9×10⁻⁷ cm²/sand 7.6×10⁻⁶ cm²/s.⁴⁸ The impedance of ion diffusion in the electrolyte can be determined by the Nernst equation:⁴⁹}

$$Z_N = (W/\sqrt{i\omega}) \tanh(\sqrt{i\omega/K_N})$$

Where *W* is the Warburg parameter and is equal to $kT/(n^2 e_0^2 C_{I_3^-} A \sqrt{D_{I_3^-}})$ and *K_N* is equal to $D_{I_3^-}/\delta^2 k$, *T*, *n* and *e₀* are the Boltzmann constant, the temperature, and the number of electrons transferred in each equation (here is equal to 2), and the elementary charge, respectively. *C*_{I₃⁻} is the concentration of I₃⁻ in the electrolyte, *A* is the electrode area, *D*_{I₃⁻} is the diffusion constant of I₃⁻ ions in the electrolyte, and *δ* is the thickness of the diffusion layer (It depends on the space between the photo-anode and counter-electrode, *l*). The reported values of *D*_{I₃⁻} in an electrolyte with acetonitrile solvent and TPA⁺ and Li⁺ cations are 1.1 × 10⁻⁵ and 1.5 × 10⁻⁵ cm²/s, respectively.⁴⁹ For a given *D*_{I₃⁻}, *C*_{I₃⁻} and *l*, the limiting current density (*J*_{lim}) of DSC is estimated by:^{49,50}

$$J_{lim} = (2ne_0 D_{I_3^-} C_{I_3^-} N_A / l)$$

In this report, *C*_{I₃⁻} is 30mM. For the limiting current density of 20 mA/cm², the calculated distance is about 87 μm and for the limiting current density of 10 mA/cm², it is about 174 μm. These estimations demonstrate that the lateral electrode spacing below 50 μm should make no limitation in the ionic current. In this scale producing patterns using photolithography is not difficult.

Here in this research, patterned FTO, Ni, Cu, and Cr thin films were tried as the conducting electrodes for the anode and cathode. Patterning FTO using wet-etching (chemical or electrochemical etching) does not produce sharp patterns and occasionally reduced Sn lines remain around the pattern, as shown in Fig S1-a, b.

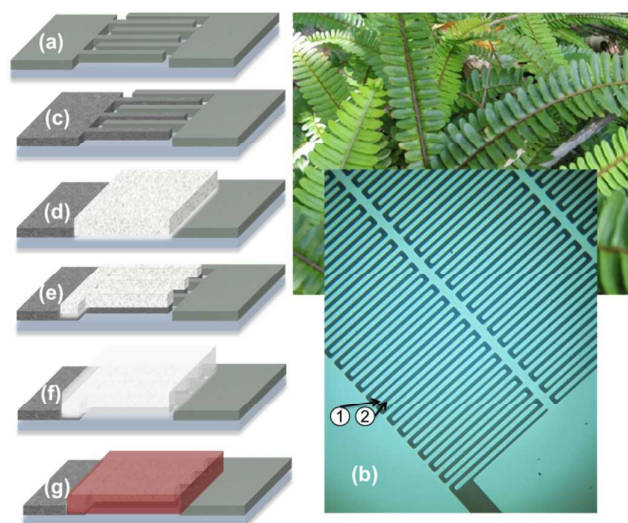


Fig. 1 (a) Schematic and (b) optical microscopy image of patterned Cr layer on the glass substrate (The thickness is about 200nm and is deposited using thermal physical vapor deposition. The pattern is produced using contact photolithography method.), and schematic of depositing procedure of different layers of the cell: (c) Pt-electrodeposition on the bracken-like substrate of counter-electrode, (d) Depositing ceramic spacer layer on both of electrodes using doctor blading method and sintering, (e) electrochemically patterning ceramic spacer layer, (f) doctor blading transparent titania paste on the pattern and sintering, and (g) dye loading.

Besides, the sheet resistance of FTO is relatively high, compared to metals, and may increase the series resistance of the fabricated device. The over-etching of FTO and high resistivity can be compensated by metal electrodeposition (e.g. Ni) over FTO pattern, as shown in Fig. S1-c, d and Fig. S2. The problem is that short contacting between photo-anode and counter-electrode is probable, due to the rapid electrodeposition of Ni (Fig S2) on the parts of the pattern that has lower sheet resistance. Patterning of Ni on the glass to make the electrodes is also challenging because cracks are developed at the edges of the pattern (Fig S3). This can be due to the poor adherence of Ni on the glass. In contrast, patterning of Cr on the glass results in sharp lines, as a result of its high adhesion to glass substrate (Fig 1-b, Fig. 2-a, Fig. S3-b and Fig. S4). The good adhesion of Cr on glass makes it possible to use electrochemical deposition method for selective deposition.

The patterned thin Cr layer must be thickened using electrodeposition for removing natural oxide layer from its surface, decreasing series resistance of the layer and increasing surface roughness and also effective surface area of the electrode (Fig. 2-b and S5). Rate of deposition is different in different parts of the bracken-like substrate according to shape and so electrical field. As stated earlier, Cr is a stable metal in the corrosive electrolyte of DSC.^{23, 24}

In order to prepare the counter-electrode, Pt layer should be deposited selectively on only one of the bracken-like electrodes.

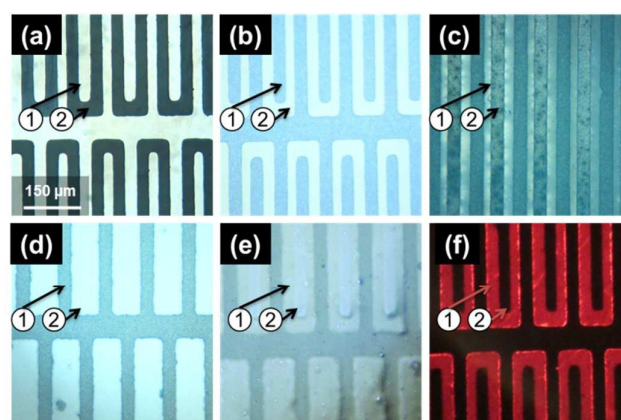


Fig. 2 Schemes for sequential deposited layers of single sided DSC: (a) Patterned thin Cr layer with thickness about 200nm (using contact photolithography method) (b) Thickened Cr layer (using Cr electrodeposition method.) (c) Pt electrodeposited bracken-like counter-electrode.(using cyclic electrodeposition method) (d) Patterned mesoporous TiO₂ spacer layer on the bracken-like counter-electrode, (e) TiO₂ transparent layer that is deposited using doctor-blading method before and (f) after dye loading. In each image, No. 1, 2 and 3 show bracken-like substrate of counter-electrode, space between photo-anode and counter-electrode and bracken-like substrate of counter-electrode.

Two approaches are possible; first is depositing Pt over the entire patterned layer (both of electrodes) and then covering Pt nanoparticles on the photo-anode electrode using Cr electrodeposition. In this approach, conventional thermal deposition or chemical reduction deposition methods are applicable. These methods have disadvantages of the probability of short-contacting bracken-like photo-anode and counter-electrode due to a nanoparticles accumulation in one point between the patterned electrodes. For this approach, the safest method is printing Pt paste. The organic part of paste prevents an accumulation of Pt nanoparticles on one point. Another approach is using electrochemical Pt deposition on one of the patterned electrodes. The uniform Pt deposition on the entire counter-electrode substrate is an essential requirement for producing a good solar cell. Pt grown structures on the electrode using constant voltage deposition method are shown in Fig 3. Density and shape of particles are different in different parts of the patterned electrode due to a different electric field, current density and defect density in different parts of the pattern. In the electrodeposition method using constant voltage, an initial number of nuclei is formed and then further growth proceeds via the present nuclei. The surface reaction at these nuclei is very fast, hence the deposition process continues in the diffusion-controlled regime, and no further new nuclei are created. The concentration of initial nuclei is higher at the end of each electrode branch, due to higher current density. This leads to non-uniform deposition over the electrode. To overcome this problem we used a cyclic electrodeposition method. In this method, as we have already reported,²⁴ the deposition near the cation reduction potential (-0.6 V relative to Ag/AgCl) is not diffusion controlled, therefore in each cycle, the number of nuclei will be increased and new nuclei will be created, resulting in more

ARTICLE

PCCP

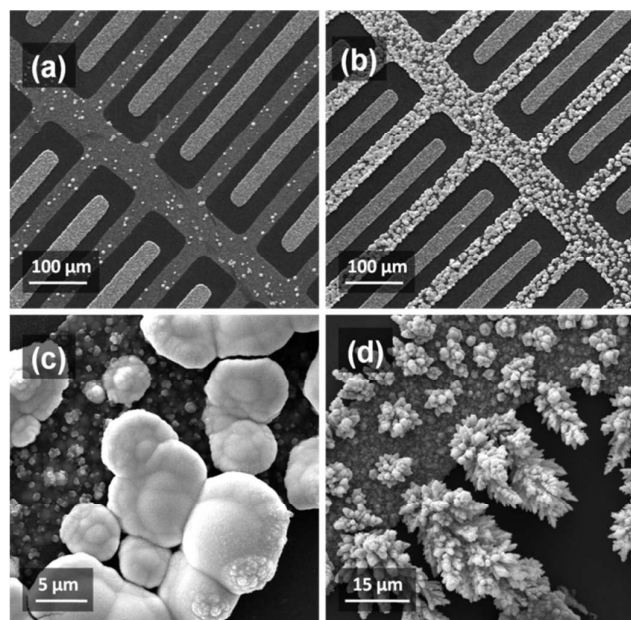


Fig.3 SEM images of different morphologies of Pt particles on the bracken-like counter-electrode for deposition time of 500s (a) and 4000s (b,c and d). Morphology of deposited Pt is different in different parts of the electrode due to different local current density. The solution contained 3mM H_2PtCl_6 and 50mM KCl in water and deposition done in room temperature (25°C) with voltage of 0V relative to Ag/AgCl electrode.

uniform deposition, as shown in Fig. 2-c. We have already shown that in case of deposition of Pt nanoparticles on a non-patterned substrate using cyclic electrochemical deposition, Pt nanoparticles are smaller and the density of Pt nanoparticles is higher compared to constant voltage method. For the optimum deposition condition, we used a solution of 3mM H_2PtCl_6 and 50mM KNO_3 in water, and the bath temperature of $40\text{--}65^\circ\text{C}$. To prevent from producing a short circuit between the counter-electrode and photo-anode, we used 1, 3 and 8 cycles of electrodeposition (Probability of short-contacting increases with increasing the number of cycles).

In this structure, substrates of electrodes are separated horizontally, TiO_2 mesoporous layer must be deposited using doctor-blading method and will cover the entire of both of electrodes, so there must be a uniform separating insulator layer or void, to keep the TiO_2 film from short-contact with the underlying counter-electrode. This is one of the most challenging problems with this patterned DSC structure.

Several methods were tried to create a vertical separation of TiO_2 and Pt electrodes. One approach is depositing a uniform sacrificial layer on the Pt/Cr bracken-like electrode. After deposition and sintering the TiO_2 mesoporous layer, this sacrificial layer is removed to create an empty space between Pt electrode and TiO_2 film. Polyaniline, Cu and ZnO layers were tried due to easy depositing procedures for making a uniform sacrificial layer. Polyaniline was deposited with excellent uniformity (Fig S6), however, it has the problem that it should be heated up to 500°C to be removed.

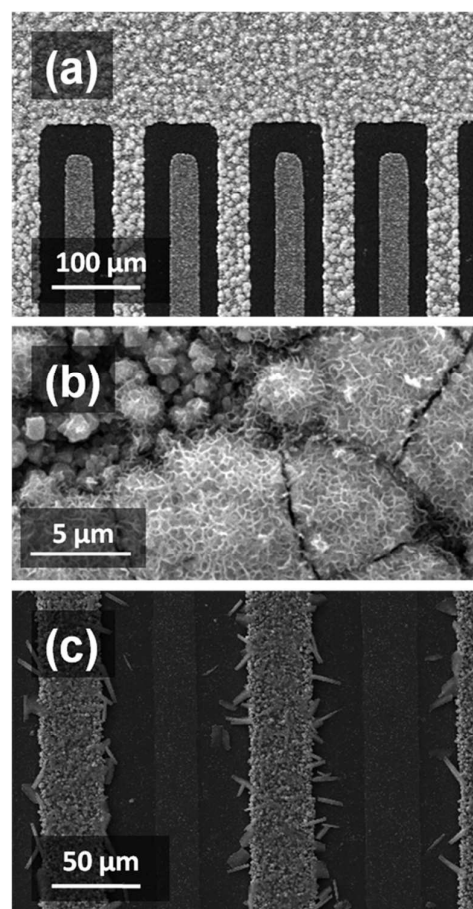


Fig.4 SEM images of different morphologies of deposited ZnO layer on the Pt counter-electrodes using constant voltage (a & b) and cyclic (c) electrodeposition method. In the constant voltage deposition procedure, the voltage is -0.72V respect to Ag/AgCl reference electrode, bath temperature is 60°C , and deposition time is 1500s. The deposition time for depositing Pt nanoparticles before ZnO deposition is 2000s using constant voltage that is described in Fig. 3. The Pt nanoparticles prevent from producing continuous layer of ZnO on the surface.

In this temperature, the oxide layer on the metallic substrate will be thickened and will produce high internal resistance in the cell^{23,24} (Fig S7). Cu layer can be deposited easily and can be removed using nitric acid (Fig S8) without etching Cr substrate (nitric acid forms a Cr_2O_3 layer), but this chemical dissolution process may pollute the TiO_2 film (hence increasing recombination). Besides, the growth rate of Cu is not well controllable (Fig S9). Growth of metal oxide layers such as ZnO is more controllable (Fig S10). We tried to electrodeposit ZnO layer as a sacrificial layer on the Pt/Cr bracken-like electrode, as ZnO can be easily removed without contaminating the TiO_2 layer. SEM images of ZnO deposited electrode are shown in Fig. S10 (c and d). For this sample, Pt and ZnO nuclei are deposited with constant voltage relative to Ag/AgCl reference electrode. Pt is not deposited uniformly, so ZnO is not deposited uniformly on

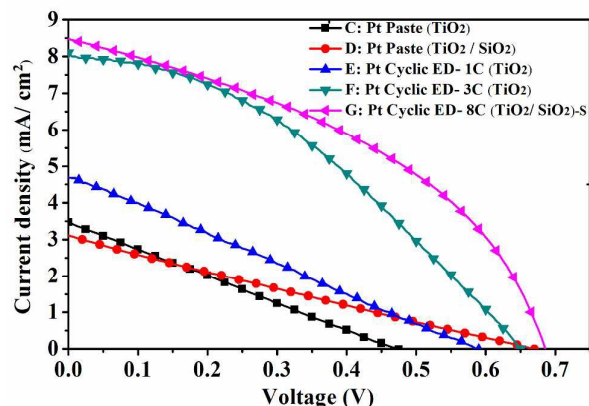


Fig. 5 Current density/ Voltage curve for different monolithic bracken like DSCs with different counter-electrodes (prepared using Pt paste deposition procedure or Pt electrodepositing procedure for different number of deposition cycles and using TiO_2 or $\text{TiO}_2/\text{SiO}_2$ particulate layer as a porous spacer layer). One notes that Pt paste deposition leads to low performance compared to the cyclic electrodeposition. Comparing the TiO_2 and $\text{TiO}_2/\text{SiO}_2$ spacer layer, the latter results in considerably better V_{oc} values. In the figure, "Pt Paste" and "Pt Cyclic ED" refer to Pt counter-electrode deposition using paste deposition or cyclic electrodeposition. (TiO_2) or ($\text{TiO}_2/\text{SiO}_2$) represent the particles used as the spacer layer. The symbol "S" refers to using Titania sol spin-coating for depositing a thin layer of titania compact layer on the substrate of photo-anode to prevent from thickening the oxide layer.

the entire bracken-like electrode subsequently. This poor coverage will produce a short circuit in a DSC device. In the case of ZnO deposition using cyclic electrodeposition, ZnO rods are produced instead of a compact layer as shown in Fig. 4-c. This may be due to apply Pt nanoparticles as a catalyst that directs the current into certain points on the surface, leading to rod-like structures.

We finally developed a different approach that is, creating a porous spacer layer selectively on the counter-electrode. For this purpose, a porous layer of TiO_2 is deposited over the entire anode and cathode electrodes using doctor blade method, followed by sintering. The deposited layer on the photo-anode will be removed by applying a negative voltage to the counter-electrode in Cr bath deposition solution. The released gas over the photo-anode electrode caused removing the TiO_2 porous layer, while at the same time, the deposition of Cr layer proceeds instead (Fig. 2-d). Conventional insulator spacer layer that is used for monolithic DSC structures is a mesoporous ZrO_2 layer.¹⁸ In the current case, the size of particles in the paste and the consistency of the prepared meso-porous layer are very important. The TiO_2 porous layer with the particle size of 150-250nm is a proper choice. These particles are not too large to collapse during the release of gas in Cr deposition on the photo-anode (only TiO_2 layer around the photo-anode bracken-like electrode substrate must be removed) and are not too small to adsorb significant amount of dye molecules. DSC devices with the mentioned fabrication procedures were prepared. The device performance for a collection of various conditions is demonstrated in Table 1 and Fig. 5.

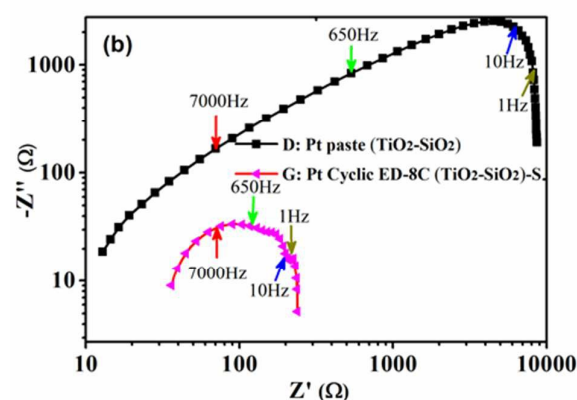
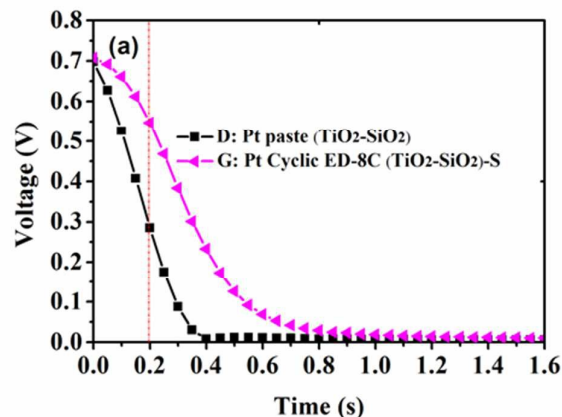


Fig. 6 Open circuit voltage decay (a) for bracken-like monolithic devices with counter-electrodes prepared by doctor blading a Pt paste (device D) and by cyclic electrochemical depositing (8 cycles- device G) and their EIS curves (b). The spacer layer for both samples is $\text{TiO}_2/\text{SiO}_2$ particulate layer. For Pt paste deposition, the voltage decay is clearly faster compared to the electrodeposited Pt. One notes a considerably lower device resistance for the DSC with electrodeposited counter-electrode (G).

Among the preparation methods for the Pt counter-electrode, the conventional thermal decomposition method (drop casting of H_2PtCl_4) results in no device output, due to making short contacting between the electrodes (device A, Table 1). Short contacting and device failure also occurs for Pt deposition using chemical reduction method (device B, Table 1).

The failures for these liquid drop methods might be due to better wetting of the substrate compared to the Cr electrodes that eventually creates considerable Pt deposit on the spacing between the bracken-like electrodes. The wetting problem can be partially improved by using a Pt paste instead of a liquid drop (device C). Pt paste is deposited using Dr blade method and the Pt content of the paste is deposited after thermal treatment. As shown in Fig. 5, the device using Pt paste deposition exhibits non-zero output, however, the values of J_{sc} and V_{oc} are small ($3.47\text{mA}/\text{cm}^2$ and 0.475V).

Table 1 The performance for the DSC devices fabricated using bracken-like metal electrodes. The effect of different preparation methods for Pt counter-electrode deposition, as well as different spacer layers is demonstrated.

Sample name	Type of Pt deposition	Spacer	Treatment	J_{sc} (mA/cm ²)	V_{oc} (V)	FF	η (%)
A	Thermal Pt deposition (drop casting)						
B	Low temperature chemical Pt deposition using ethylene glycol		Short circuit between the electrodes				
C	Thermal Pt deposition (doctor blading 3wt% Pt paste)	TiO ₂ (100-250 nm)	—	3.47	0.475	0.25	0.41
D	Thermal Pt deposition (doctor blading 3wt% Pt paste)	TiO ₂ /SiO ₂ (100-250 nm/50nm)	—	3.12	0.670	0.24	0.50
E	Cyclic Pt electrodeposition (1 cycle)	TiO ₂ (100-250 nm)	—	4.69	0.590	0.26	0.71
F	Cyclic Pt electrodeposition (3 cycle)	TiO ₂ (100-250 nm)	—	8.10	0.660	0.35	1.88
G	Cyclic Pt electrodeposition (8 cycle)	TiO ₂ /SiO ₂ (100-250 nm/50nm)	1wt% TiO ₂ sol spin coating	8.47	0.685	0.41	2.44

Besides, the fill factor is poor (0.25). These are indications of a high recombination rate in the device. As already discussed, Pt paste deposition is not perfect in terms of avoiding any current leak paths between the two bracken-like electrodes; while it is clearly better than drop methods.

For the mentioned Pt paste sample (device C), TiO₂ sub-micron particles were used as the porous spacer layer. While TiO₂ possesses good electron transport properties, we assumed that the photo-anode and cathode electrodes cannot “see” each other through the TiO₂ spacer layer, due to the limited diffusion length of the electrons. This assumption is not completely true; the device performance is improved if an insulated TiO₂/SiO₂ composite layer is used as the spacer layer (device D). By TiO₂/SiO₂ spacer layer, V_{oc} is largely improved, while J_{sc} is almost unchanged (device D versus C). This indicates higher electron density in the photo-anode, resulting from lower electron leakage through the TiO₂/SiO₂ spacer layer. The V_{oc} for device D is 0.67V, indicating that the TiO₂/SiO₂ layer is sufficiently good as a spacer layer.

The current density for device D (3.12mA/cm²) is still low, while V_{oc} is acceptable. The low J_{sc} , as well as fill factor, reveals that Pt paste deposition cannot provide counter-electrodes with sufficiently low charge transfer resistance. For devices E, F, and G, cyclic electrodeposition of Pt was used to prepare the counter-electrode. One of the advantages of electrodeposition is selective deposition over a single electrode, with no deposition on the other electrode or the spacing between the electrodes. For devices E, F, and G 1 cycle, 3 cycles and 8 cycles of Pt deposition were used, respectively. One notes that cyclic electrodeposition provides higher current density compared to Dr blade paste deposition. One cycle of deposition is apparently insufficient, resulting in $J_{sc} =$

4.69mA/cm². By increasing the number of cycles to 3, J_{sc} is improved to 8.10mA/cm². For 8 cycles, there is still slight current density enhancement to 8.47mA/cm². Best efficiency for this structure is achieved by using 8 cycles of Pt electrodeposition, a TiO₂/SiO₂ spacer layer, and an additional TiO₂ sol treatment prior to TiO₂ mesoporous paste deposition. This latter process, as already reported, provides lower contact resistance between the Cr substrate and TiO₂ mesoporous layer.²³ The best efficiency is 2.44%.

To compare electrodeposition and paste blading methods for Pt electrode deposition, the device D and device G (Pt Paste deposited and 8 cycles electrodeposited plus both TiO₂/SiO₂ spacer layer) were compared using open circuit voltage decay (Fig. 6a) and electrochemical impedance spectroscopy (Fig. 6b). The slope of the V_{oc} decay curve is an indication of the recombination time.²³ As observed in Fig. 6a, the timescale for the V_{oc} to reach 50% of the initial value is 0.17sec and 0.32sec for device D (Paste deposition) and device G (electrodeposition). These are very long compared to the lifetime in conventional DSCs. In open circuit DSCs, the photoelectrons transferred into the TiO₂ body, eventually recombine with the redox species in the electrolyte, either through the surface of the TiO₂ mesoporous layer or through the FTO substrate. Recombination from the substrate is usually dominant, hence, a thin TiO₂ blocking layer (e.g. by TiCl₄ treatment) is applied on the FTO surface to control the recombination. If the blocking layer is thick (e.g. 100nm), then the charge is trapped for a long time and V_{oc} decays very slowly.⁵¹

In this single sided Cr electrode DSC, the very slow V_{oc} decay is possibly due to the formation of a blocking chromium oxide film. The oxide layer on chromium is formed during the high-

temperature treatments after Pt paste and TiO₂ paste depositions. Therefore, the oxide film exists for both Dr blade Pt and electrodeposited Pt devices. As shown in Fig. 6a, V_{oc} decays faster for device D, where Pt is deposited by Dr blading a Pt paste. This can be a result of Pt residue that remains under the TiO₂ mesoporous layer. These metal nanoparticles can act as recombination centers. Fig. 6b is the EIS plots of the same devices. Fitting results with details are reported in Fig S11&S12 and Table S1. The impedance values are about two orders of magnitude different; hence the curves are plotted in the log-log representation. We already have investigated the EIS of Cr-based DSCs for photo-anode and also counter-electrode. For the photoanode, we showed that the EIS curve can be fitted by a few semicircles: a semi-circle in the frequency of about 7000Hz related to charge transfer at the interface of counter-electrode and the electrolyte, a semi-circle in the frequency of about 10Hz related to the charge transfer at the interface of the nano-porous titania layer and the electrolyte, and a semicircle in a frequency about 650 Hz due to the interfacial oxide layer on the chromium layer and the upper-layer (in the case of using chromium as a substrate for photo-anode, this semi-circle is related to chromium oxide and titania interfacial layer and in the case of using chromium as a substrate for counter-electrode it is related to chromium oxide and Pt interfacial layer).²³ The impedance of ion-diffusion in the electrolyte appears in frequencies lower than 1Hz. These frequencies are indicated in EIS curves of D and G devices in comparison with each other. In case of device D, a large semicircle is observed that we attribute to the interfacial resistance due to chromium oxide layer. The thicker oxide film on Cr electrodes is expected for device D compared to device G, as an additional thermal treatment is required for Pt deposition from a paste.

Experimental

The fabrication steps are summarized in Fig. 1 and Fig. 2. The steps are described as follows:

1. Preparing patterned bracken like substrate

Patterning Cr layer. The thin Cr layer with a thickness of about 200 nm, deposited by PVD method on a glass substrate, was patterned using a home-made contact photolithography setup (Shipley photoresist S-1400) as shown in Fig. 1-a, 1-b, and 2-a. NaOH solution (5g/l) was used as a developer solution and a solution containing 1.2g Ce(NO₃)₆(NH₄)₂ and 1ml CH₃COOH in 9ml DI water as a Cr etching solution. To decrease the electrical resistance of both electrodes, the layers were thickened by electrodepositing Cr layer (solution containing 210g/l CrO₃ and 2.1g/l H₂SO₄ in DI water). The current density and deposition times were 60 mA and 1 min. We used a mask using scotch tape around the pattern to confine depositing first on the pattern and then the mask is removed for depositing on the pattern and the outside. The layers were immersed in DI water right after the electrodeposition.

Patterning Ni layer. The thin Ni layer with a thickness of about 200 nm (deposited using PVD method on a glass substrate) was patterned using a similar mentioned, however with an etching solution containing nitric acid, sulphuric acid, and DI water with 1: 1: 3 relative concentration.

Patterning FTO layer. The FTO layer on the glass was patterned using chemical and electrochemical methods. In both cases, photoresist layer which is deposited on the FTO surface is patterned using contact photolithography. In the chemical method, Zn powder (Merck) is spread on the surface and adding a solution of 3.3M HCl in DI water to the FTO surface causes FTO etching. In the electrochemical method, The FTO with patterned photoresist on its surface is placed as a cathode (stainless steel as the anode) in a two-electrode cell containing 1 M HCl as the electrolyte by applying -0.6 V to the FTO electrode.

2. Deposition of Pt nanoparticles

Thermal and chemical reduction methods. In case of thermal deposition, a drop of 5mM H₂PtCl₆.6H₂O in 2-propanol is spread on the patterned bracken-like structure, followed by heating at 400 °C for 20min. Chemical reduction is carried out by drop casting ethylene glycol/H₂PtCl₆ in 2-propanol solution with 1: 1 volume percentage on a hot patterned substrate, which is placed on a hotplate with temperature of 120 °C. After evaporation of solvent, the substrate will be darker due to Pt nanoparticles deposition.

Doctor blade method. A 3mM H₂PtCl₆.6H₂O paste (Sharif Solar) and 40 μm thick tape were used for doctor-blading the paste over the whole pattern. The layer was heated up to 300 °C for 10 min for removing organic parts of the paste.

Electrochemical deposition method. Electrochemical Pt deposition is carried out via a three-electrode system with Ag/AgCl electrode as a reference electrode, Pt deposited FTO as a counter-electrode and the masked patterned chromium/glass (one of its bracken-like electrodes) as the working electrode (Fig. 1-c). Pt solution contained 3mM H₂PtCl₆ and 50mM KNO₃. For deposition with constant voltage, the selected voltage was 0 V relative to Ag/AgCl reference electrode and deposition time was 500s, 2000s and 4000s, and the deposition temperature was 25 °C. For depositing via cyclic deposition 1, 3 and 8 deposition cycles were chosen and the deposition temperature was 40 °C. In both cases, Pt electrodeposition was performed right after Cr electrodeposition to avoid formation of nanometric natural Cr₂O₃ layer.

3. Deposition of the spacer layer

Different materials such as Cu, polyaniline and ZnO were examined for electro-deposition on the Pt deposited bracken-like counter-electrode as a separating layer, protecting the counter-electrode from short contact with the TiO₂ photo-anode electrode (Fig. 1-d).

Polyaniline deposition. The deposition solution contained 4mM sulphuric acid and 5.5mM aniline in DI water. The electrodeposition was carried out using a three electrode system, Ag/AgCl as the reference electrode, stainless steel as the counter-electrode and the bracken-like Pt electrode as the working electrode. The voltage was scanned from -0.3V to 0.9V with a scan rate of 0.05V/s.

Cu electrodeposition. Cu film was deposited using a two-electrode system. The solution contained 1M Cu₂SO₄.6H₂O and 0.6M H₂SO₄ in water. The bath temperature was 25 °C.

ZnO electrodeposition. The Solution used for ZnO deposition contained 0.1M Zn(NO₃)₂ in water. The Deposition was performed using a three-electrode system with Ag/AgCl reference electrode and a stainless steel foil as the counter-electrode. The deposition

time, temperature of the bath and the selected voltage were 1500 s, 60 °C, and -0.72V.

After doctor blading TiO₂ paste on the spacer layer and sintering, the ZnO or Cu layer can be removed by immersing in diluted nitric acid. The Cr layer would not be damaged in nitric acid.

Doctor blading TiO₂ composite as a spacer layer. 20wt% TiO₂ scattering paste or 20 wt% TiO₂/SiO₂(1:4) scattering paste was used as a porous spacer layer. 0.4 g of these pastes were diluted by 1 g ethanol and deposited by spin coating. A lift-off electrochemical method was used for depositing the TiO₂ scattering layer selectively on one of bracken-like electrodes as a spacer layer by applying negative voltage to the photo-anode. The hydrogen evolved in this process *cleans* the surface of photo-anode from the TiO₂ paste and leaves TiO₂ spacer layer only on the Pt electrode. After depositing Pt nanoparticles on one of the bracken-like electrodes, the scattering paste was deposited using doctor blading method, then sintered at 500 °C for 30 min. Cr layer was deposited with a very low current density (200-320 mA/cm²) on the photo-anode bracken-like electrode substrate to remove TiO₂ layer around it and deposit a fresh Cr layer on it. The current density should be low enough to restrain from removing TiO₂ coating on the counter-electrode.

4. Fabricating single-sided bracken-like DSCs

12wt% transparent paste of TiO₂ nanoparticles with 20nm in diameter (Sharif Solar) is used for dye adsorbing mesoporous TiO₂ layer. The transparent TiO₂ layer with a thickness about 8µm was then deposited on the entire pattern and then sintered in 450 °C for about 20min. The layer was immersed in a 0.2mM solution of N719 dye solution (cis- di(thiocynato)-N,N0-bis (2,20-bipyridyl-4-carboxylic acid-40-tetrabutylammonium carboxylate)) ruthenium(II) , Dyesol) prepared in 1:1 acetonitrile/tertiary butanol (Merck) solution for about 18 h (Fig.1-f) following by rinsing by acetonitrile.

The prepared structure was sealed using a piece of glass and surlyn spacer layer (with thickness of 60µm) and filled with I⁻/ I₃⁻ electrolyte containing 30mM I₂, 100mM LiI, 0.6M TBAI and 500mM TBP in acetonitrile solvent.

5. Characterization

The current density-voltage curve was measured under AM1.5 illumination conditions (Sharif Solar Solar simulator) using Palmsens potentiostat. OCVD measurement is done using three 10W white LEDs. EIS measurement (100mHz-100kHz) is done using Autolab instrument. Light and electron microscope images were taken using Jenus-IE200M and Vega Tescan machine, respectively.

Conclusions

A novel metal-based, FTO-free single sided DSC is introduced in this work. Two laterally separated patterned electrodes are created using photolithography and different solution-based deposition methods. For Pt deposition, it is found that the conventional drop casting methods leads to short contacting the electrodes. Dr blade deposition using a Pt paste, and electrodeposition can be successfully used. We found a cyclic electrodeposition method is the most optimum deposition method, as it creates selective

deposit on a single electrode at room temperature and provides better device efficiency. Another challenge of this patterned single sided DSC structure is the formation of a spacer layer that keeps anode-cathode from short contact. Cu and ZnO sacrificial layers were not successful, as in both cases depositing uniform layers by electrodeposition was challenging. A problem in this regards is the selective electrodeposition on the already existing Pt nanoparticles on the electrodes, which inhibit the formation of a layered dense film. Porous layers of TiO₂ and TiO₂/SiO₂ sub-micron particles worked well as the spacer layer while TiO₂/SiO₂ showed better device performance due to higher resistivity. A novel method of selective porous spacer deposition is used where TiO₂ (or TiO₂/SiO₂) paste is first deposited all over the surface and then the part on the anode electrode is lift off by electrodeposition of Cr on the anode electrode. Cr electrodeposition produces bubbles that remove the porous spacer layer.

Best devices show 2.24% efficiency which is still low compared to conventional DSCs. V_{oc} decay curves of the devices show very slow decay that demonstrates the formation of a chromium oxide blocking layer over the Cr substrate. This layer is formed during the thermal treatments (after Pt or TiO₂ paste depositions). The effect of this blocking layer is increasing the internal device resistivity, as confirmed by EIS analysis, and decreasing fill factor. Further process optimization is required in order to avoid thick chromium oxide, by low-temperature TiO₂ deposition. It should be noted that the conventional DSCs are sandwich type structures that need two substrates linked together using a thermo-plastic sealant. The manufacturing of two-sided cells is, in principle, more complex than single-sided cells. Besides, in the conventional two-sided cells, the distance between the electrodes is determined by the spacer layer which is dependent on how the two sides are sandwiched together, while in single-sided cells the distance between the electrodes is the same.

References

- 1 B. E. Hardin, H. J. Snaith and M. D. McGehee, *Nat. Photonics*, 2012, **6**, 162–169.
- 2 M. Toivola, F. Ahlskog and P. Lund, *Sol. Energy Mater. Sol. Cells*, 2006, **90**, 2881–2893.
- 3 K. Miettunen, J. Halme, M. Toivola and P. Lund, *J. Phys. Chem. C*, 2008, **112**, 4011–4017.
- 4 T. Ma, X. Fang, M. Akiyama, K. Inoue, H. Noma and E. Abe, *J. Electroanal. Chem.*, 2004, **574**, 77–83.
- 5 C. M. Chen, C. H. Chen and T. C. Wei, *Electrochim. Acta*, 2010, **55**, 1687–1695.
- 6 T. N. Murakami and M. Grätzel, *Inorganica Chim. Acta*, 2008, **361**, 572–580.
- 7 H. Chang, T. L. Chen, K. D. Huang, S. H. Chien and K. C. Hung, *J. Alloys Compd.*, 2010, **504**, S435–S438.

PCCP	ARTICLE
8 Y. Jun, J. Kim and M. G. Kang, <i>Sol. Energy Mater. Sol. Cells</i> , 2007, 91 , 779–784.	27 S. H. Kim and C. W. Park, <i>Bull. Korean Chem. Soc.</i> , 2013, 34 , 831–836.
9 M. G. Kang, N.-G. Park, K. S. Ryu, S. H. Chang and K.-J. Kim, <i>Sol. Energy Mater. Sol. Cells</i> , 2006, 90 , 574–581.	28 J. L. Lan, Y. Y. Wang, C. C. Wan, T. C. Wei, H. P. Feng, C. Peng, H. P. Cheng, Y. H. Chang and W. C. Hsu, <i>Curr. Appl. Phys.</i> , 2010, 10 , S168–S171.
10 K. Onoda, S. Ngamsinlapasathian, T. Fujieda and S. Yoshikawa, <i>Sol. Energy Mater. Sol. Cells</i> , 2007, 91 , 1176–1181.	29 L. Chen, W. Tan, J. Zhang, X. Zhou, X. Zhang and Y. Lin, <i>Electrochim. Acta</i> , 2010, 55 , 3721–3726.
11 X. Fan, F. Wang, Z. Chu, L. Chen, C. Zhang and D. Zou, <i>Appl. Phys. Lett.</i> , 2007, 90 , 99–101.	30 X. Fang, T. Ma, G. Guan, M. Akiyama, T. Kida and E. Abe, <i>J. Electroanal. Chem.</i> , 2004, 570 , 257–263.
12 X. Huang, P. Shen, B. Zhao, X. Feng, S. Jiang, H. Chen, H. Li and S. Tan, <i>Sol. Energy Mater. Sol. Cells</i> , 2010, 94 , 1005–1010.	31 Y. L. Lee, C. L. Chen, L. W. Chong, C. H. Chen, Y. F. Liu and C. F. Chi, <i>Electrochem. commun.</i> , 2010, 12 , 1662–1665.
13 Z. Liu, V. R. Subramania and M. Misra, <i>J. Phys. Chem. C</i> , 2009, 113 , 14028–14033.	32 H.-J. K. H.-J. Kim, Y.-C. K. Y.-C. Kim, I.-G. L. I.-G. Lee, J.-T. H. J.-T. Hong, D.-Y. L. D.-Y. Lee and J.-Y. C. J.-Y. Choi, <i>2006 Int. Symp. Discharges Electr. Insul. Vac.</i> , 2006, 2 , 48–51.
14 D. Fu, P. Lay and U. Bach, <i>Energy Environ. Sci.</i> , 2013, 6 , 824–829.	33 C. H. Tsai, S. Y. Hsu, C. Y. Lu, Y. T. Tsai, T. W. Huang, Y. F. Chen, Y. H. Jhang and C. C. Wu, <i>Org. Electron. physics, Mater. Appl.</i> , 2012, 13 , 199–205.
15 K. Okada, H. Matsui, T. Kawashima, T. Ezure and N. Tanabe, <i>J. Photochem. Photobiol. A Chem.</i> , 2004, 164 , 193–198.	34 G. Tsekouras, A. J. Mozer and G. G. Wallace, <i>J. Electrochem. Soc.</i> , 2008, 155 , K124–K128.
16 H. Wang, Y. Liu, H. Xu, X. Dong, H. Shen, Y. Wang and H. Yang, <i>Renew. Energy</i> , 2009, 34 , 1635–1638.	35 L.-L. Li, C.-W. Chang, H.-H. Wu, J.-W. Shiu, P.-T. Wu and E. Wei-Guang Diau, <i>J. Mater. Chem.</i> , 2012, 22 , 6267.
17 H. Pettersson, T. Gruszecki, L. H. Johansson and P. Johander, <i>Sol. Energy Mater. Sol. Cells</i> , 2003, 77 , 405–413.	36 D. Fu, P. Huang and U. Bach, <i>Electrochim. Acta</i> , 2012, 77 , 121–127.
18 S. Ito and K. Takahashi, <i>Int. J. Photoenergy</i> , 2012.	37 S. S. Kim, Y. C. Nah, Y. Y. Noh, J. Jo and D. Y. Kim, <i>Electrochim. Acta</i> , 2006, 51 , 3814–3819.
19 S. J. Thompson, J. M. Pringle, X. L. Zhang and Y.-B. Cheng, <i>J. Phys. D. Appl. Phys.</i> , 2013, 46 , 024007.	38 P. Li, J. Wu, J. Lin, M. Huang, Y. Huang and Q. Li, <i>Sol. Energy</i> , 2009, 83 , 845–849.
20 J. Kwon, N.-G. Park, J. Y. Lee, M. J. Ko and J. H. Park, <i>ACS Appl. Mater. Interfaces</i> , 2013, 5 , 2070–2074.	39 K. C. Huang, Y. C. Wang, P. Y. Chen, Y. H. Lai, J. H. Huang, Y. H. Chen, R. X. Dong, C. W. Chu, J. J. Lin and K. C. Ho, <i>J. Power Sources</i> , 2012, 203 , 274–281.
21 N. Fuke, A. Fukui, R. Komiya, A. Islam, M. Yanagida, R. Yamanaka, L. Han and Y. Chiba, 2008, 4974–4979.	40 M. Sun and X. Cui, <i>J. Power Sources</i> , 2013, 223 , 74–78.
22 N. Fuke, R. Katoh, A. Islam, M. Kasuya, A. Furube, A. Fukui, Y. Chiba, R. Komiya, R. Yamanaka, L. Han and H. Harima, <i>Energy Environ. Sci.</i> , 2009, 2 , 1205–1209.	41 P.-J. Li, K. Chen, Y.-F. Chen, Z.-G. Wang, X. Hao, J.-B. Liu, J.-R. He and W.-L. Zhang, <i>Chinese Phys. B</i> , 2012, 21 , 118101.
23 F. Behrouznejad and N. Taghavinia, <i>ChemElectroChem</i> , 2014, 1 , 944–950.	42 V. Tjoa, J. Chua, S. S. Pramana, J. Wei, S. G. Mhaisalkar and N. Mathews, <i>ACS Appl. Mater. Interfaces</i> , 2012, 4 , 3447–3452.
24 F. Behrouznejad and N. Taghavinia, <i>J. Power Sources</i> , 2014, 260 , 299–306.	43 H. S. Jang, J. M. Yun, D. Y. Kim, S. I. Na and S. S. Kim, <i>Surf. Coatings Technol.</i> , 2014, 242 , 8–13.
25 D. Fu, X. Li Zhang, R. L. Barber and U. Bach, <i>Adv. Mater.</i> , 2010, 22 , 4270–4274.	44 Z. Tang, J. Wu, M. Zheng, Q. Tang, Q. Liu, J. Lin and J. Wang, <i>RSC Adv.</i> , 2012, 2 , 5034–5037.
26 M. Wu, T. Ma, <i>J. Phys. Chem. C</i> , 2014, 118 , 16727–16742.	

ARTICLE

PCCP

- 45 M.Y. Yen, C. C. Teng, M. C. Hsiao, P. I. Liu, W. P. Chuang, C. C. M. Ma, C. K. Hsieh, M. C. Tsai and C. H. Tsai, *J. Mater. Chem.*, 2011, **21**, 12880-12888.
- 46 C.-T. Liu, Y.-C. Wang, R.-X. Dong, C.-C. Wang, K.-C. Huang, R. Vittal, K.-C. Ho and J.-J. Lin, *J. Mater. Chem.*, 2012, 25311–25315.
- 47 M. Law, L. E. Greene, J. C. Johnson, R. Saykally and P. Yang, *Nat. Mater.*, 2005, **4**, 455–459.
- 48 A. Hagfeldt, G. Boschloo, L. Kloo and H. Pettersson, *Chem. Rev.*, 2010, **110**, 6595–6663.
- 49 a. Hauch and a. Georg, *Electrochim. Acta*, 2001, **46**, 3457–3466.
- 50 B. li, *Instrumental Methods in Electrochemistry Questions* :, 2011.
- 51 P. J. Cameron, L. M. Peter and S. Hore, *J. Phys. Chem. B*, 2005, **109**, 930–936.